

See discussions, stats, and author profiles for this publication at: <https://www.researchgate.net/publication/267742560>

Two-Dimensional Π -Expanded Quinoidal Terthiophenes Terminated with Dicyanomethylenes as n-Type Semiconductors for High-Performance Organic Thin-Film Transistors.

ARTICLE in JOURNAL OF THE AMERICAN CHEMICAL SOCIETY · OCTOBER 2014

Impact Factor: 12.11 · DOI: 10.1021/ja510003y · Source: PubMed

CITATIONS

12

READS

34

7 AUTHORS, INCLUDING:



[Yaping Zang](#)

Chinese Academy of Sciences

13 PUBLICATIONS 55 CITATIONS

[SEE PROFILE](#)



[Eliot Gann](#)

Monash University (Australia)

52 PUBLICATIONS 935 CITATIONS

[SEE PROFILE](#)



[Christopher R. McNeill](#)

Monash University (Australia)

112 PUBLICATIONS 3,697 CITATIONS

[SEE PROFILE](#)



[Chong-an Di](#)

Chinese Academy of Sciences

109 PUBLICATIONS 3,651 CITATIONS

[SEE PROFILE](#)

Two-Dimensional π -Expanded Quinoidal Terthiophenes Terminated with Dicyanomethylenes as n-Type Semiconductors for High-Performance Organic Thin-Film Transistors

Cheng Zhang,^{†,‡} Yaping Zang,^{†,‡} Eliot Gann,^{§,||} Christopher R. McNeill,^{||} Xiaozhang Zhu,^{*,†}
Chong-an Di,^{*,†} and Daoben Zhu[†]

[†]Beijing National Laboratory for Molecular Sciences, CAS Key Laboratory of Organic Solids, Institute of Chemistry, Chinese Academy of Sciences, Beijing 100190, P. R. China

[‡]University of Chinese Academy of Sciences, Beijing 100049, P. R. China

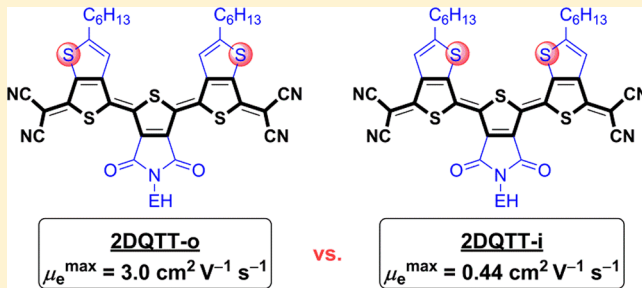
[§]Australian Synchrotron, 800 Blackburn Road, Clayton, Victoria 3168, Australia

^{||}Department of Materials Engineering, Monash University, Clayton, Victoria 3800, Australia

S Supporting Information

ABSTRACT: Quinoidal oligothiophenes (**QOT**), as classical n-type semiconductors, have been well-known for a long time but with non-optimal semiconducting properties. We report here the design and selective synthesis of new two-dimensional (2D) π -expanded quinoidal terthiophenes, **2DQTTs**, with proximal (**2DQTT-i**) and distal (**2DQTT-o**) regiochemistry for high-performance n-channel organic thin-film transistors (n-OTFTs) featuring high electron mobility, solution processability, and ambient stability. The elegant combination of thieno[3,4-*b*]thiophene [TT, donor (D)] and 5-alkyl-4H-thieno[3,4-*c*]pyrrole-4,6(5H)-dione [TPD, acceptor (A)] units

with relatively large π -surface endows these **2DQTTs** with distinctive 2D structural characteristics and flat configuration stabilized by weak intramolecular S–O/S weak interactions. Furthermore, the A–D–A–D–A electronic structure maintains an adequately low LUMO energy level. These **2DQTTs** are shown to exhibit outstanding semiconducting properties with electron mobilities of up to $3.0 \text{ cm}^2 \text{ V}^{-1} \text{ s}^{-1}$ and on/off ratios of up to 10^6 (**2DQTT-o**) in ambient- and solution-processed OTFTs. Investigations on thin-film morphology reveal that the microstructure of **2DQTTs** is highly dependent on the orientation of the fused thiophene subunits, leading to differences in electron mobilities of 1 order of magnitude. X-ray diffraction studies in particular reveal increased crystallinity, crystalline coherence, and orientational order in **2DQTT-o** compared to **2DQTT-i**, which accounts for the superior electron transport property of **2DQTT-o**.



2DQTT-o

$$\mu_e^{\max} = 3.0 \text{ cm}^2 \text{ V}^{-1} \text{ s}^{-1}$$

vs.

2DQTT-i

$$\mu_e^{\max} = 0.44 \text{ cm}^2 \text{ V}^{-1} \text{ s}^{-1}$$

INTRODUCTION

For n-type organic semiconductors,¹ control of the lowest unoccupied molecular orbital (LUMO) energy level is a prerequisite for ambient-stable n-channel organic thin-film transistors (n-OTFTs),² which has contributed to the sluggish development of this technology. Among various types of n-type organic semiconductors reported, quinoidal oligothiophenes (**QOTs**)³ have been recognized as promising n-type semiconductors with appropriate LUMO energy levels (<−3.9 eV vs the vacuum level) derived from the quinoidal molecular structure terminated by two strongly electron-withdrawing dicyanomethylenes. Considerable efforts have been made to develop new **QOTs** for high-performance OTFTs, by means of improving solubility⁴ and enhancing intermolecular interactions by utilizing fused thiophene frameworks⁵ or incorporating selenophene units.⁶ However, despite over 10 years of explorations,^{3a} the electron mobilities of **QOTs** are still lower than $1.0 \text{ cm}^2 \text{ V}^{-1} \text{ s}^{-1}$, the median value of amorphous silicon, which makes them

apparently less promising than state-of-the-art rylene diimides.⁷

Compared with perylene dimide (PDIs) derivatives⁸ with large polycyclic aromatic hydrocarbon (PAH) cores, linear **QOTs** show a smaller π -surface, which may negatively affect the magnitude of the transfer integral, an important factor for charge transport in organic semiconductors.⁹ The mobility bottleneck of **QOTs** might be solved by overcoming the key issue of limited π – π intermolecular stacking related to their linear molecular structure. Thus, we selected thieno[3,4-*b*]thiophene¹⁰ and 5-alkyl-4H-thieno[3,4-*c*]pyrrole-4,6(5H)-dione¹¹ units with relatively large π -surfaces for the construction of new 2D π -expanded quinoidal terthiophenes, **2DQTT-i** and **2DQTT-o** (Figure 1). Besides the expanded conjugation surfaces for better intermolecular π – π interaction,¹² the combination of TT

Received: June 26, 2014

Published: October 28, 2014

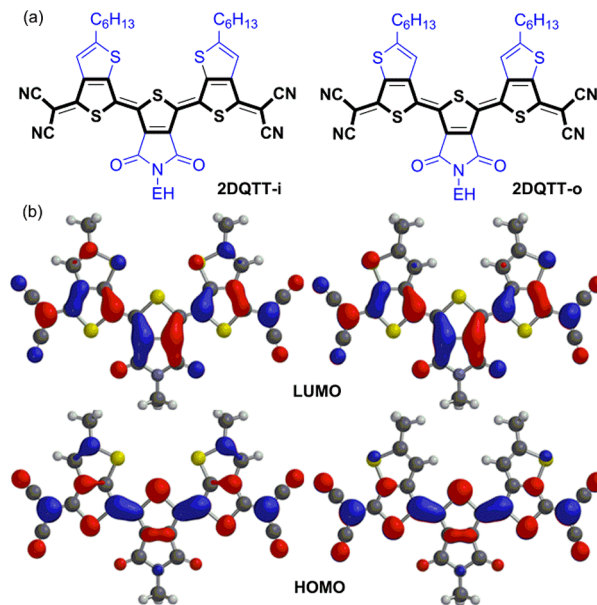


Figure 1. Molecular structures (a), optimized geometry and HOMO/LUMO orbitals of 2DQTT-i and 2DQTT-o (b) (EH = 2-ethylhexyl). (Calculations were conducted at the DFT//B3LYP/6-31G* level. Alkyl substituents were replaced by methyl groups to simplify the calculations.)

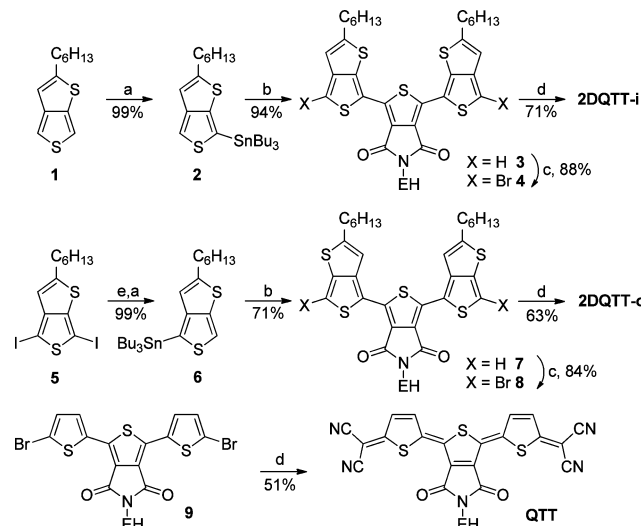
and TPD units endows the molecules with additional distinct structural characteristics: (1) The flat configuration can be stabilized by weak intramolecular S–O and/or S (lateral thiophene)–S (central thiophene) interactions;¹³ (2) the A–D–A–D–A electronic structure can keep the LUMO levels adequately low; (3) the alkyl substituents of TPD units provide additional opportunities for tuning solubility and thin-film morphology of the semiconducting layer based on 2DQTTs in OTFTs.¹⁴

We report herein the design and selective synthesis of new 2D π -expanded quinoidal terthiophenes, 2DQTT-i and 2DQTT-o (Figure 1), for high-performance n-type OTFTs featuring high electron mobility, solution processability, and ambient stability. Both compounds showed electron mobilities of over 10^{-1} cm² V⁻¹ s⁻¹. Intriguingly, we find that the observed electron mobilities are highly dependent on the orientation of two fused TT subunits with a significant difference of 1 order of magnitude. OTFT devices based on 2DQTT-o gave high electron mobilities of up to 3.0 cm² V⁻¹ s⁻¹ with current on/off ratios from about 10^5 to 10^6 , revealing the great potential of 2DQOT framework for applications in n-type organic semiconductors.

RESULTS AND DISCUSSION

Synthesis of 2DQTTs. The selective synthesis of 2DQTT-i and 2DQTT-o is shown in Scheme 1. Interestingly, deprotonation of TT¹⁵ by *n*-butyllithium at -78 °C in THF occurred exclusively at the 6-position and after addition of tributyltin chloride gave tributyl(2-hexylthieno[3,4-*b*]thiophen-6-yl)stannane 2 in 99% yield. The Stille coupling reaction between compound 2 and 1,3-dibromo-5-(2-ethylhexyl)-4H-thieno[3,4-*c*]pyrrole-4,6(SH)-dione (TPD-2Br) afforded compound 3 in excellent yield of 94%. After bromination of compound 3, compound 4 was obtained and subjected to Pd-catalyzed coupling with sodium dicyanomethanide followed by DDQ oxidation to give 2DQTT-i as a brick-red solid in 71% yield. Compound 2 was synthesized through a similar

Scheme 1. Selective Synthesis of Compounds 2DQTT-i, 2DQTT-o, and QTT^a



^aReagents and conditions: (a) (i) *n*-BuLi, THF, -78 °C; (ii) tributyltin chloride; (b) TPD-2Br, Pd(PPh₃)₄, toluene/DMF, 90 °C; (c) NBS, DMF/CHCl₃, rt; (d) (i) malonitrile, NaH, Pd(PPh₃)₄, 1,4-dioxane, 100 °C; (ii) HCl, DDQ, rt; (e) (i) *n*-BuLi, THF, -78 °C; (ii) H₂O.

procedure. The key intermediate tributyl(2-hexylthieno[3,4-*b*]thiophen-4-yl)stannane 6 was obtained from 2-hexyl-4-iodothieno[3,4-*b*]thiophene, which could be synthesized by the highly selective Li–I exchange reaction between 2-hexyl-4,6-diiodothieno[3,4-*b*]thiophene 5 and *n*-butyllithium at the 6-position of TT followed by a second Li–I exchange at the 2-position. The selective deprotonation or Li–I exchange reactions at the 6-position of TT might be individually ascribed to the high acidity or Li–S interaction from the adjacent sulfur atoms. The reference quinoidal terthiophene (QTT) without fused thiophene units was also synthesized for comparison. 2DQTT-i, 2DQTT-o, and QTT showed good thermal stability (up to 290, 306, and 357 °C, respectively, at which 5 wt % loss was recorded, see Supporting Information) and ample solubility in CHCl₃ (about 15 mg/mL) at room temperature (rt), which guaranteed solution-based fabrication of OTFT devices.

2DQTT-i and 2DQTT-o were fully characterized by conventional NMR and mass and elemental analysis. The ¹H NMR spectrum of 2DQTT-i showed a single peak in the aromatic region, δ 7.66 ppm, which can be assigned to β -hydrogens of the two equivalent fused thiophene subunits, and remained unchanged in deuterated chloroform for days, which indicated the absence of an isomerization process.¹⁶ From the theoretical calculation at the B3LYP/6-31G* level (Figure 1b), we found that 2DQTT-i had a planar molecular structure with short multiple O–S and S–S interactions with distances of 2.898 Å for O–S and 3.204 Å for S–S, which were smaller than the sum of O, S (3.32 Å) and S, S (3.60 Å) van der Waals radii. However, for 2DQTT-o, we observed two groups of signals in the aromatic region, which suggested the existence of two stereoisomers because of the reduced intramolecular interactions. The main isomer with a single peak at 7.28 ppm was assigned to the molecular structure with an *E,E*-configuration in the terthienoquinoidal core as shown in Figure 1a. The other isomer had two signals at 7.31 and 7.66 ppm, which we assigned to an *E,Z*-configuration in the terthienoquinoidal core.

The ratio of two stereoisomers was determined to be 86:14 based on the integration of the related hydrogen signals. Because the isomer ratios did not change after recrystallizing the products three times, we deduced that the isomers existed in the solution as a thermodynamic equilibrium. During the growth of single crystals, we found that only very thin flake crystals could be obtained for **2DQTT-i**, which were proved to be twin crystals and were not suitable for X-ray structural analysis. After numerous attempts, single crystals of **2DQTT-o** were finally obtained that were suitable for X-ray analysis from mixed dichloromethane/ethyl acetate solvent. Although the single crystal of **2DQTT-o** was measured at the low temperature, 113 K, to prevent unfavorable effects from the molecular vibration, we could not obtain clear diffraction points of the carbon atoms in the alkyl chains, and instead, dispersive ones were observed. To solve this problem, we limited the location of carbon atoms of the alkyl chains manually by the isotropic method, which resulted in a relatively large R value (0.17). Fortunately, the diffraction from the conjugated backbone could be easily confirmed and treated by the anisotropy method, and we did not find any errors from the conjugated backbone. The *E,E*-configuration of **2DQTT-o** is shown in Figure 2. **2DQTT-o** is almost planar with a small torsional

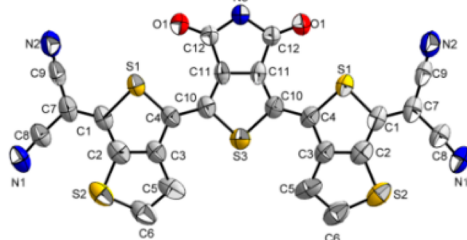


Figure 2. Molecular structures of **2DQTT-o** with 50% probability ellipsoids. (The alkyl chains are omitted for clarity.)

angle of 5.27°. The short distance S–O contact (2.834 Å), which can be clearly observed, is very close to the calculated value (2.850 Å) obtained from the theoretically optimized structure and contributes to the planar molecular structure.¹³ Combining the suitable side chains attached on the conjugated backbone, *n*-hexyl groups at the 2-position of TTs and 2-ethylhexyl groups on the TPD, **2DQTT-o** shows a packing mode of “brick-layer” arrangement (Figure S5–S8) with impact slipped π – π intermolecular interactions of 3.441 Å, which is different from the herringbone packing of the classical linear quinoidal terthiophenes.^{3a}

Absorption and Electrochemical Properties of 2DQTTs.

The physical properties of **2DQTT-i** and **2DQTT-o** in diluted dichloromethane solution and thin films were investigated. Both compounds show intense near-infrared absorptions at 774 nm (**2DQTT-i**) and 750 nm (**2DQTT-o**) as shown in Figure 3. Compared with that in solution, the maximum absorption of **2DQTT-o** in film was significantly bathochromically shifted to 952 nm by 202 nm, which suggests the existence of a *J*-aggregation, an encouraging indication for favorable electron transfer in thin-film devices.¹⁷ By contrast, the absorption band of **2DQTT-i** in thin film simply became broadened, but still with a comparable absorption maximum at 782 nm. Thus, the aggregation patterns of **2DQTT-i** and **2DQTT-o** in thin films should be different, which accordingly could result in differing OTFT performance. Because of the quinoidal

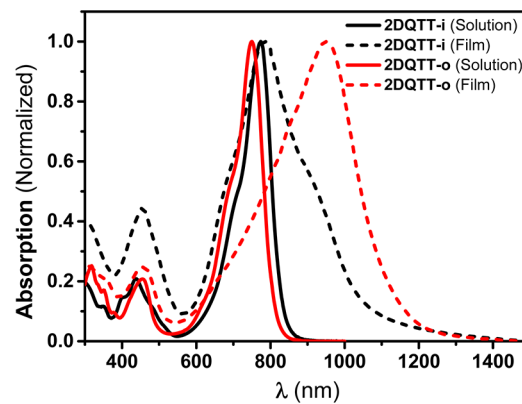


Figure 3. Absorption spectra of **2DQTT-i** (black) and **2DQTT-o** (red) in dichloromethane (solid lines) and thin-film states (dashed lines).

backbones, both compounds had two reduction processes, but the first reduction of **2DQTT-i** was irreversible (see Supporting Information). The LUMO energy levels are estimated to be –4.77 eV for **2DQTT-i**, –4.51 eV for **2DQTT-o**, and –4.75 eV for QTT by the empirical equation, $LUMO = -(4.80 + E_{onset})$ eV (E_{onset} : the onset of the reduction wave). Although both compounds are very stable in ambient solution and solid state, **2DQTT-o** should be more suitable to be applied as a stable n-type semiconductor because of its favorable LUMO energy level.¹⁸

Thin-Film Transistor Characterization of 2DQTTs and QTT.

The potential of **2DQTT-i** and **2DQTT-o** for use in n-type OTFTs was investigated. Bottom-gate bottom-contact (BGBC) OTFT devices were fabricated on octadecyltrichlorosilane (OTS)-modified SiO_2 (300 nm)/Si substrates. Thin films (40–60 nm in thickness) were spin-coated as the organic semiconducting layer, and 30 nm gold served as the source–drain electrodes. The thin films were annealed at 80, 120, 160, 190, or 240 °C. Figure 4 shows the I – V characteristics of **2DQTT-i** and **2DQTT-o**. All the devices exhibit similar characteristics in air and under N_2 atmosphere, probably as a result of the deep LUMO energy level, with well-defined linear and saturation regimes. The device performances of **2DQTT-i** and **2DQTT-o** were collected and are summarized in Table 1. Devices based on **2DQTT-i** show a stepwise improvement of electron mobility with increasing annealing temperature ($\mu_{e(\text{avg})} = 0.03 \text{ cm}^2 \text{ V}^{-1} \text{ s}^{-1}$ at 80 °C; and $\mu_{e(\text{avg})} = 0.14 \text{ cm}^2 \text{ V}^{-1} \text{ s}^{-1}$ at 190 °C). A maximum mobility of $0.44 \text{ cm}^2 \text{ V}^{-1} \text{ s}^{-1}$ was observed for an annealing temperature of 190 °C. **2DQTT-o**-based devices display a different trend compared with OTFTs based on **2DQTT-i**. No obvious increase in mobility was observed after annealing at a temperature lower than 120 °C. However, the mobility increased significantly from $0.05 \text{ cm}^2 \text{ V}^{-1} \text{ s}^{-1}$ to a value well over $1.5 \text{ cm}^2 \text{ V}^{-1} \text{ s}^{-1}$ after annealing at 160 °C. An exciting device performance with a maximum electron mobility of $3.0 \text{ cm}^2 \text{ V}^{-1} \text{ s}^{-1}$ and $I_{\text{on}}/I_{\text{off}} = 10^5$ was achieved.¹⁹ This performance makes **2DQTT-o** one of the best solution-processable air-stable n-channel semiconductors. By sharp contrast, QTT shows inferior electron mobilities, by as much as 4 orders of magnitude. Figure 5 shows the histograms of the electron mobility distribution for 24 OTFTs based on **2DQTT-i** and **2DQTT-o**, respectively. For **2DQTT-i**-based transistors most devices display moderate mobility higher than $0.1 \text{ cm}^2 \text{ V}^{-1} \text{ s}^{-1}$. As a comparison, all the OTFTs based **2DQTT-o** exhibit electron mobility higher than $0.8 \text{ cm}^2 \text{ V}^{-1} \text{ s}^{-1}$,

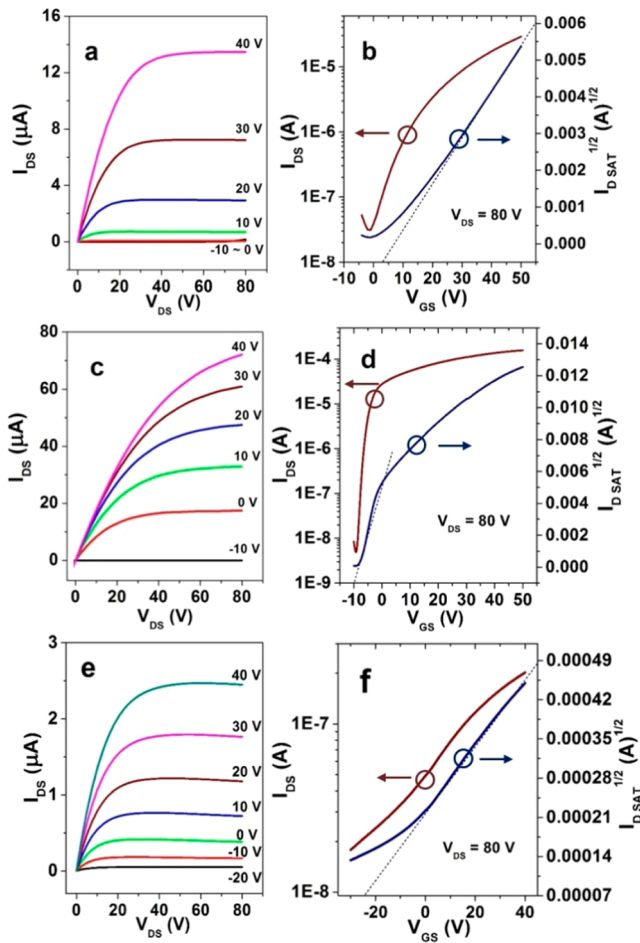


Figure 4. Output (a, c, e) and transfer (b, d, f) characteristics of BGBC OTFTs based on 2DQTT-i (a, b), 2DQTT-o (c, d), and QTT (e, f). Devices based on 2DQTT-i and 2DQTT-o were annealed at 190 and 160 °C, respectively.

while 25% devices show mobility higher than $2.0 \text{ cm}^2 \text{ V}^{-1} \text{ s}^{-1}$. From these data we can meaningfully conclude that 2DQTT-o possesses superior charge transport than that of 2DQTT-i.²⁰ These results indicate that the orientation of the two fused TT subunits and balanced 2D structure have a significant influence on the carrier transport properties.

Thin-Film Morphology. To explore the annealing temperature-dependent performances of 2DQTT-i- and 2DQTT-o-based

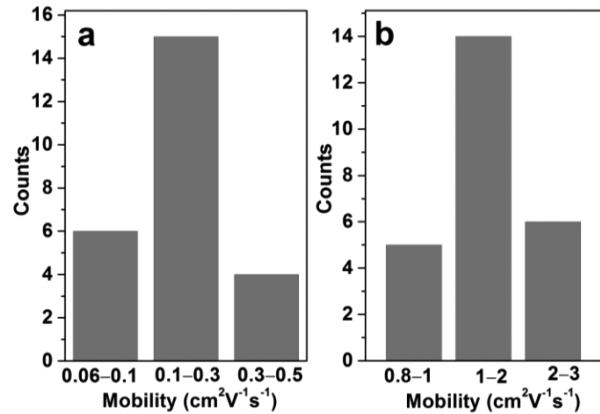


Figure 5. Histograms of device mobility for a set of OFETs based on 2DQTT-i (a) and 2DQTT-o (b), composed of 24 separate devices.

OTFTs, thin films of 2DQTT-i and 2DQTT-o were examined by atomic force microscopy (AFM) measurements. Figure 6 shows the AFM images of spin-coated films annealed at different temperatures (from 80 to 190 °C). No obvious change of film morphology of 2DQTT-i was observed after annealing at a temperature lower than 160 °C, but enhanced lamellar ordering was observed after annealing at 190 °C. By comparison with the film morphology of the 2DQTT-i, the 2DQTT-o-based films appeared more crystalline with larger, more obvious domains that grow in size with increasing annealing temperature. An ordered film with large grain size (200–1000 nm) and terraced surface microstructure can be successfully obtained when annealed at 160 °C.

The two-dimensional grazing incidence wide-angle X-ray scattering (2D GIWAXS) images for 2DQTT-i and 2DQTT-o as a function of annealing temperature are shown in Figure 7. 2D GIWAXS investigations are consistent with our AFM studies. Out-of plane GIWAXS patterns of spin-coated thin films at room temperature indicated strong first-order diffraction peaks with similar 2θ values of 4.93° (2DQTT-o) and 5.06° (2DQTT-i), which correspond to d -spacing of 17.9 and 17.5 Å, respectively. With increasing annealing temperature, the first-order diffraction peak became more intense with a higher-order diffraction peak observed at 9.8° , indicating increasing crystallinity of the thin films, contributing to the outstanding performances obtained under high annealing temperatures. Increasing annealing temperature results in a greater enhancement of lamellar peak intensity in films of 2DQTT-o than that

Table 1. Maximum (Average) Electron Mobilities (μ_e)^a, Current On/Off Ratios (I_{on}/I_{off}), and Minimum (Average) Threshold Voltages (V_{Th}) for OTFT Devices Based on 2DQTT-i, 2DQTT-o, and QTT

semiconductor	annealing temperature (°C)	electron mobility (μ_e) ($\text{cm}^2 \text{ V}^{-1} \text{ s}^{-1}$)	I_{on}/I_{off}	V_{Th} (V)
2DQTT-i	80	0.05 (0.03)	10^3 (10^3)	2.1 (6.4)
	120	0.05 (0.04)	10^3 (10^3)	0.8 (6.4)
	160	0.21 (0.1)	10^3 (10^3)	3.6 (9.3)
	190	0.44 (0.14)	10^3 (10^3)	2.6 (5.4)
	240	0.14 (0.1)	10^3 (10^3)	2.1 (8.7)
2DQTT-o	80	0.14 (0.05)	10^6 (10^5)	-15.2 (-19.8)
	120	0.12 (0.05)	10^4 (10^4)	-19.8 (-23)
	160	3.0 (1.51)	10^6 (10^5)	-1.4 (-11.1)
	190	0.74 (0.43)	10^6 (10^5)	-6.9 (-11)
QTT	80	0.0002 (0.0005)	10^2 (10^2)	-10.0 (-31.0)
	120	0.0003 (0.0005)	10 (10)	-26.3 (-52.1)

^aTypical device characteristics obtained from 25 devices; all devices were measured under ambient conditions.

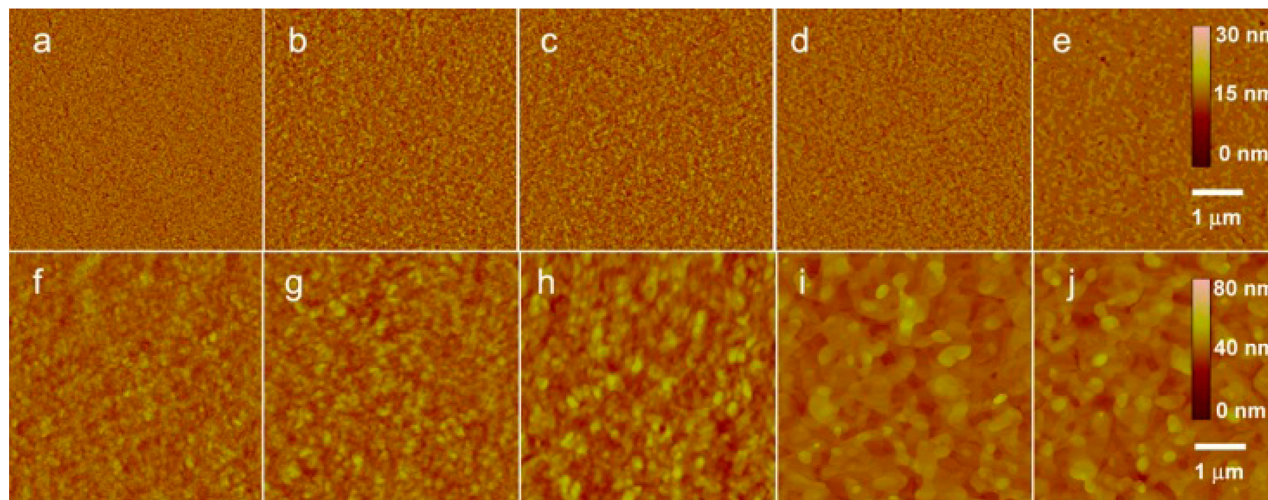


Figure 6. AFM images of thin films of **2DQTT-i** and **2DQTT-o** at room temperature (a, f) and after thermal annealing at temperatures of 80 °C (b, g), 120 °C (c, h), 160 °C (d, i), and 190 °C (e, j), respectively. (Upper panels: **2DQTT-i**, lower panels: **2DQTT-o**.)

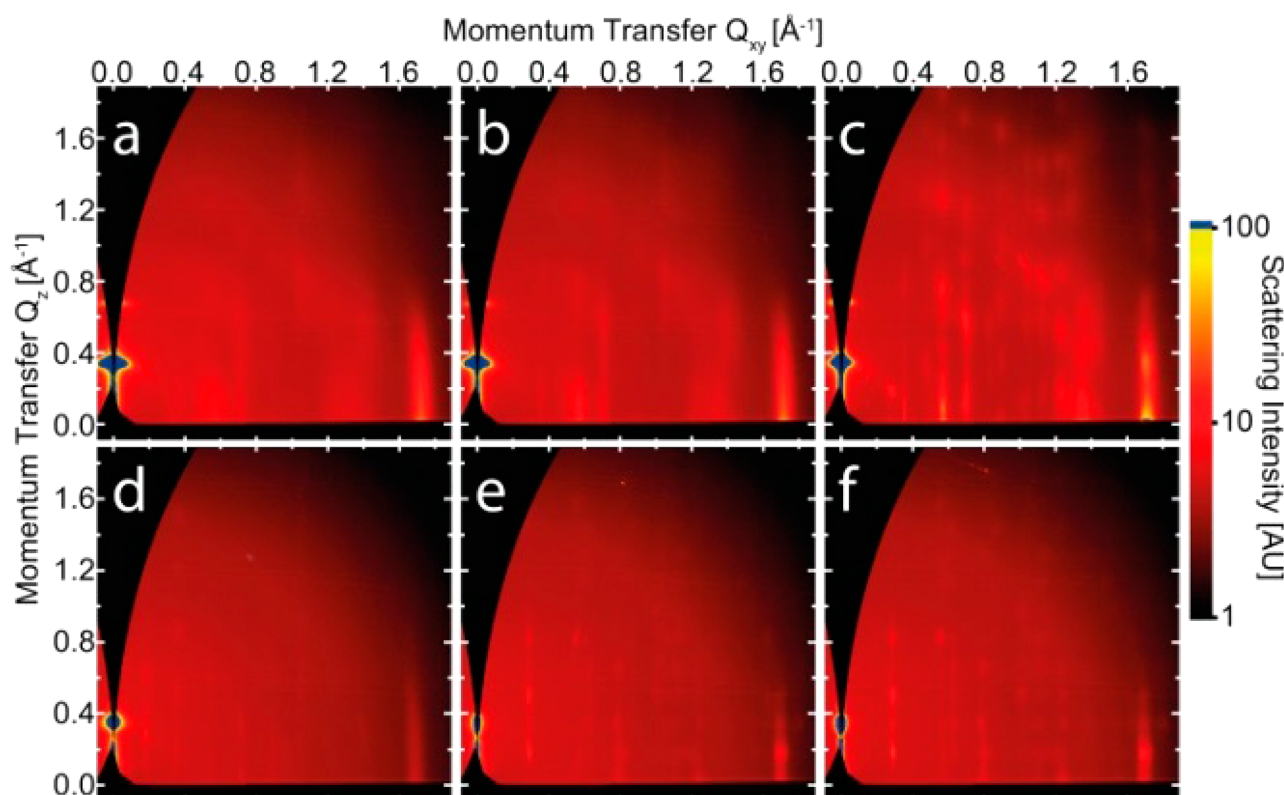


Figure 7. 2D GIWAXS patterns of **2DQTT-i** and **2DQTT-o** at different annealing temperatures of 120 °C (a, d), 160 °C (b, e), and 190 °C (c, f), respectively.

of **2DQTT-i**. By sharp contrast, X-ray diffraction (XRD) measurements of **QTT** (Figure S9) indicate amorphous aggregation of **QTT**, which may be responsible for the inferior OTFT performance. All of the results indicate varied crystalline properties of **QTT** derivatives induced by sulfur position in the molecules. 2D GIWAXS in addition collects the off-specular diffraction, importantly including the in-plane direction critical for charge transport in OTFTs, and the orientational width of each peak. Both **2DQTT-i** and **2DQTT-o** stack edge-on to the substrate with strongest reflections corresponding to alkyl stacking perpendicular to the substrate and a peak located

in-plane at about 1.7 \AA^{-1} which likely corresponds to $\pi-\pi$ stacking. With annealing, **2DQTT-i** largely maintains a single-crystal structure, the peaks of which become more intense, indicating an increase in overall crystallinity, and sharper, indicating an increased crystalline coherence length or larger crystals with annealing. The orientational full width at half-maximum (fwhm) of **2DQTT-i** steadily decreases from 6.4° at 120 °C to 4.3° and 190 °C. For **2DQTT-o** there exists a clear unit cell change with annealing from 120 to 160 °C (also observed in the corresponding AFM images) and increasing crystallinity with annealing to 190 °C. The orientational fwhm

decreases from 5.5° at 120 °C to 3.4° at both 160 and 190 °C. Compared with **2DQTT-i**, **2DQTT-o** shows much sharper peaks, indicative of larger crystalline coherence lengths and this higher degree of orientational order. Assuming the intense peak located in-plane at about 1.7 Å⁻¹ can be assigned to π–π stacking, we evaluate a π–π cofacial stacking distance of 3.4 Å for both compounds which is largely in agreement with the value from the single-crystal analysis of **2DQTT-o** discussed above. In summary, minor differences in the molecular structure of **2DQTT-i** and **2DQTT-o** significantly affect the molecular packing and thin-film morphology, which results in disparate OTFT performance.

Discussion. The construction of **2DQTTs** was successfully realized by the selective functionalization of unsymmetrical TT unit. The weak O–S and S–S intramolecular interactions resulted in **2DQTT-i** with exclusive *E,E*-configuration. Because of the absence of S–S interactions, a minor amount of the **2DQTT-o** isomer with *E,Z*-configuration can be visible in solution state in ¹H NMR spectrum. However, **2DQTT-o** showed exclusively the *E,E*-configuration in solid state as indicated by single-crystal X-ray analysis. Differing from the herringbone packing of linear QOTs, **2DQTT-o** showed favorable “brick-layer” arrangement²¹ in bulk single-crystal state because of the expanded π-surface¹² and steric hindrance²² of the branched 2-ethylhexyl groups attached on the central TPD unit. J-aggregation of **2DQTT-o** was clearly observed in the thin film revealing the slipped molecular arrangement. The LUMO energy level of **2DQTT-o** is proper (−4.51 eV) as a stable n-type semiconductor.

For typical organic semiconductor-based OTFTs, the carrier transport is mainly determined by the intermolecular charge transport inside the crystalline domains and the carrier trapping in the intergrain regions. As indicated by AFM images (Figure 6) and 2D GIWAXS (Figure 7), obvious differences in film morphology of **2DQTT-i** and **2DQTT-o** were observed. **2DQTT-o** film possesses larger domain size and crystalline coherence length when the annealing temperature reached 160 °C than that of **2DQTT-i** under same condition. In addition, the intermolecular stacking plays an important role in determining the device performances. With the aid of 2D GIWAXS measurements, we are able to gain further insight into the packing mode of **2DQTTs** in thin films. For many solution-processed organic semiconductors, different crystalline forms can exist, but single crystals of different phases are difficult to obtain.²³ In this case, although we obtained single crystals of **2DQTT-o**, we find the molecular packing extracted from the obtained single crystal does not match the intermolecular stacking seen in thin film by GIWAXS. The unit cells of **2DQTT-i** and **2DQTT-o** were calculated by fitting diffraction peaks and scattering backgrounds using a Levenberg–Marquardt nonlinear least-squares fitting method. **2DQTT-i** largely maintains the same crystal structure with annealing (with optimized unit cell parameters $a = 19$ Å, $b = 17.5$ Å, $c = 11.25$ Å, $\alpha = 90^\circ$, $\beta = 80^\circ$, $\gamma = 83^\circ$) with annealing leading to increasing crystalline coherence length (8.74 nm, 190 °C) and overall level of crystallinity. At 190 °C, however, a second minority crystal form with unidentified but much larger unit cell is also visible in the GIWAXS pattern from **2DQTT-i**, indicating a partial phase transition between 160 and 190 °C. (Figure S10). The optimized unit cell parameters of **2DQTT-o** ($a = 11.3$ Å, $b = 37.5$ Å, $c = 21.54$ Å, $\alpha = 90^\circ$, $\beta = 90^\circ$, $\gamma = 90^\circ$) are similar, although distinct from those found in bulk single-crystal measurements, with an approximate doubling of unit cell volume

relative to the single-crystal measurements, indicating two molecules per unit cell in the thin film. In addition, **2DQTT-o** exhibits a phase change with annealing from a yet larger, but indistinct unit cell, to that given above when annealing from 120 to 160 °C, a transition also observed in the corresponding AFM images. **2DQTT-o** increases slightly in crystallinity with further annealing to 190 °C. However, thin films of **2DQTT-o** annealed at 160 °C give a better OTFT performance compared with annealing at 190 °C. One possibility for the decrease in performance, despite an apparent microstructural improvement, might be in-plane thermal expansion,^{23b} which can produce microscopic defects when the **2DQTT-o** film was quenched from 190 °C to room temperature, but less when quenched from 160 °C. In any case, the morphology of the **2DQTT-o** thin film, with the lowest measured orientational disorder, and largest crystalline coherence length (9.89 nm) after annealing to 160 °C is most suitable for electron transfer. From OTFT characterization, **2DQTT-o** showed higher electron mobilities of up to 3.0 cm² V⁻¹ s⁻¹ than that of **2DQTT-i** by one order of magnitude. By contrast, the reference QTT with unbalanced 2D structure showed much inferior electron mobilities of low to 10⁻⁴ cm² V⁻¹ s⁻¹. Thus, for organic semiconductors with asymmetric monomer units, TT in our case, the molecular regiochemistry may significantly affect the device performance and should be paid extra attention in molecular design toward organic semiconductors with prominent charge transport properties.²⁴

CONCLUSION

In conclusion, we have developed new 2D π-expanded quinoidal terthiophenes, **2DQTT-i** and **2DQTT-o**, based on highly selective synthetic strategy. Both compounds showed distinctive 2D molecular structures with enhanced configuration stability because of the weak S–O and/or S–S intramolecular multi-interactions. Because of the A–D–A–D–A electronic structure, the LUMO energy levels of **2DQTTs** are adequately low for applications in ambient-stable n-OTFTs and gave electron mobilities at the 10⁻¹ cm² V⁻¹ s⁻¹ level. The minor change of thiophene orientation in **2DQTT-i** and **2DQTT-o** significantly affected film morphology that resulted in different OTFT performances: 0.44 cm² V⁻¹ s⁻¹ (**2DQTT-i**) compared with 3.0 cm² V⁻¹ s⁻¹ (**2DQTT-o**). Higher crystallinity, longer crystalline coherence lengths, and the lowest orientational disorder of the crystalline structure of **2DQTT-o** compared to **2DQTT-i** accounts for its superior conductivity. As the reference, QTT with unbalanced 2D structure showed much inferior electron mobilities of low to 10⁻⁴ cm² V⁻¹ s⁻¹. To the best of our knowledge, **2DQTT-o** is the first example among QOTs that exhibits an electron mobility surpassing 1.0 cm² V⁻¹ s⁻¹, revealing the potential of **2DQOT**-framework for constructing n-type organic semiconductors that can rival or even surpass state-of-the-art rylene diimides via proper molecular design.²⁵

EXPERIMENTAL SECTION

Materials and General Methods. All the reactions dealing with air- or moisture-sensitive compounds were carried out in a dry reaction vessel under a positive pressure of nitrogen. Unless stated otherwise, starting materials were obtained from Adamas, Aldrich, and J&K and were used without any further purification. Anhydrous THF, toluene, and 1,4-dioxane were distilled over Na/benzophenone prior to use. Anhydrous DMF was distilled over CaH₂ prior to use. 2-Hexylthieno-[3,4-*b*]thiophene (**1**)¹⁵, 1,3-dibromo-5-(2-ethylhexyl)-4*H*-thieno[3,4-*c*]-pyrrole-4,6(*S,H*)-dione (**3**), and 1,3-bis(5-bromothiophen-2-yl)-5-(2-ethylhexyl)-4*H*-thieno[3,4-*c*]pyrrole-4,6(*S,H*)-dione (**9**)²⁶ were prepared according to the published procedures. Hydrogen nuclear magnetic

- (6) (a) Handa, S.; Miyazaki, E.; Takimiya, K. *Chem. Commun.* **2009**, 3919. (b) Pappenfus, T. M.; Hermanson, B. J.; Helland, T. J.; Lee, G. G. W.; Drew, S. M.; Mann, K. R.; McGee, K. A.; Rasmussen, S. C. *Org. Lett.* **2008**, *10*, 1553.
- (7) (a) Gao, X.; Di, C.-a.; Hu, Y.; Yang, X.; Fan, H.; Zhang, F.; Liu, Y.; Li, H.; Zhu, D. *J. Am. Chem. Soc.* **2010**, *132*, 3697. (b) Zhan, X.; Facchetti, A.; Barlow, S.; Marks, T. J.; Ratner, M. A.; Wasielewski, M. R.; Marder, S. R. *Adv. Mater.* **2011**, *23*, 268. (c) Liu, Z.; Zhang, G.; Cai, Z.; Chen, X.; Luo, H.; Li, Y.; Wang, J.; Zhang, D. *Adv. Mater.* **2014**, *26*, 6965.
- (8) (a) Huang, C.; Barlow, S.; Marder, S. R. *J. Org. Chem.* **2011**, *76*, 2386. (b) Schmidt, R.; Oh, J. H.; Sun, Y.-S.; Deppisch, M.; Krause, A.-M.; Radacki, K.; Braunschweig, H.; Könemann, M.; Erk, P.; Bao, Z.; Würthner, F. *J. Am. Chem. Soc.* **2009**, *131*, 6215. (c) Lv, A.; Puniredd, S. R.; Zhang, J.; Li, Z.; Zhu, H.; Jiang, W.; Dong, H.; He, Y.; Jiang, L.; Li, Y.; Pisula, W.; Meng, Q.; Hu, W.; Wang, Z. *Adv. Mater.* **2012**, *24*, 2626.
- (9) Coropceanu, V.; Cornil, J.; da Silva Filho, D. A.; Olivier, Y.; Silbey, R.; Brédas. *Chem. Rev.* **2007**, *107*, 926.
- (10) Liang, Y.; Yu, L. *Acc. Chem. Res.* **2010**, *43*, 1227.
- (11) (a) Pron, A.; Berrouard, P.; Leclerc, M. *Macromol. Chem. Phys.* **2013**, *214*, 7. (b) Zou, Y.; Najari, A.; Berrouard, P.; Beaupré, S.; Badrou, R. A.; Tao, Y.; Leclerc, M. *J. Am. Chem. Soc.* **2010**, *132*, 5330. (c) Piliego, C.; Holcombe, T. W.; Douglas, J. D.; Woo, C. H.; Beaujuge, P. M.; Fréchet, J. M. J. *J. Am. Chem. Soc.* **2010**, *132*, 7595.
- (12) (a) Debije, M. G.; Piris, J.; de Haas, M. P.; Warman, J. M.; Tomovic, Z.; Simpson, C. D.; Watson, M. D.; Müllen, K. *J. Am. Chem. Soc.* **2004**, *126*, 4641. (b) Feng, X.; Marcon, V.; Pisula, W.; Hansen, M. R.; Kirkpatrick, J.; Grozema, F.; Andrienko, D.; Kremer, K.; Müllen, K. *Nat. Mater.* **2009**, *8*, 421.
- (13) (a) Jackson, N. E.; Savoie, B. M.; Kohlstedt, K. L.; de la Cruz, M. O.; Schatz, G. C.; Chen, L. X.; Ratner, M. A. *J. Am. Chem. Soc.* **2013**, *135*, 10475. (b) Pomerantz, M. *Tetrahedron Lett.* **2003**, *44*, 1563. (c) Turbiez, M.; Frère, P.; Allain, M.; Videlot, C.; Ackermann, J.; Roncali, J. *Chem.—Eur. J.* **2005**, *11*, 3742. (d) Guo, X.; Kim, F. S.; Jenekhe, S. A.; Watson, M. D. *J. Am. Chem. Soc.* **2009**, *131*, 7206. (e) Berrouard, P.; Grenier, F.; Pouliot, J.-R.; Gagnon, E.; Tessier, C.; Leclerc, M. *Org. Lett.* **2011**, *13*, 38. (f) Guo, X.; Ortiz, R. P.; Zheng, Y.; Kim, M.-G.; Zhang, S.; Hu, Y.; Lu, G.; Facchetti, A.; Marks, T. J. *J. Am. Chem. Soc.* **2011**, *133*, 13685. (g) Huang, H.; Chen, Z.; Ortiz, R. P.; Newman, C.; Usta, H.; Lou, S.; Youn, J.; Noh, Y.-Y.; Baeg, K.-J.; Chen, L. X.; Facchetti, A.; Marks, T. J. *J. Am. Chem. Soc.* **2012**, *134*, 10966. (h) Guo, X.; Zhou, N.; Lou, S. J.; Hennek, J. W.; Ortiz, R. P.; Butler, M. R.; Boudreault, P.-L. T.; Strzalka, J.; Morin, P.-O.; Leclerc, M.; Navarrete, J. T. L.; Ratner, M. A.; Chen, L. X.; Chang, R. P. H.; Facchetti, A.; Marks, T. J. *J. Am. Chem. Soc.* **2012**, *134*, 18427. (i) Guo, X.; Quinn, J.; Chen, Z.; Usta, H.; Zheng, Y.; Xia, Y.; Hennek, J. W.; Ortiz, R. P.; Marks, T. J.; Facchetti, A. *J. Am. Chem. Soc.* **2013**, *135*, 1986.
- (14) (a) Zhang, F.; Hu, Y.; Schuettfert, T.; Di, C.-a.; Gao, X.; McNeill, C. R.; Thomsen, L.; Mannsfeld, S. C. B.; Yuan, W.; Sirringhaus, H.; Zhu, D. *J. Am. Chem. Soc.* **2013**, *135*, 2338. (b) Pei, T.; Wang, J.-Y.; Pei, J. *Chem. Mater.* **2014**, *26*, 594. (c) Mei, J.; Bao, Z. *Chem. Mater.* **2014**, *26*, 604.
- (15) Patra, A.; Wijsboom, Y. H.; Leitus, G.; Bendikov, M. *Chem. Mater.* **2011**, *23*, 896.
- (16) Higuchi, H.; Nakayama, T.; Koyama, H.; Ojima, J.; Wada, T.; Sasabe, H. *Bull. Chem. Soc. Jpn.* **1995**, *68*, 2363.
- (17) (a) Würthner, F.; Kaiser, T. E.; Saha-Möller, C. R. *Angew. Chem., Int. Ed.* **2011**, *50*, 3376. (b) Gsänger, M.; Kirchner, E.; Stolte, M.; Burschka, C.; Stepanenko, V.; Pflaum, J.; Würthner, F. *J. Am. Chem. Soc.* **2014**, *136*, 2351.
- (18) (a) Usta, H.; Risko, C.; Wang, Z.; Huang, H.; Deliomeroglu, M. K.; Zhukhovitskiy, A.; Facchetti, A.; Marks, T. J. *J. Am. Chem. Soc.* **2009**, *131*, 5586. (b) Ye, Q.; Chang, J.; Huang, K.-W.; Shi, X.; Wu, J.; Chi, C. *Org. Lett.* **2013**, *15*, 1194.
- (19) As the factors influencing threshold voltages are quite varied, we preliminarily attribute the different threshold voltages to the different packing patterns of 2DQTT-i and 2DQTT-o; see: Veres, J.; Ogier, S.; Lloyd, G.; de Leeuw, D. *Chem. Mater.* **2004**, *16*, 4543.
- (20) Luber, E. J.; Buriak, J. M. *ACS Nano* **2013**, *7*, 4708.
- (21) Dong, H.; Fu, X.; Liu, J.; Wang, Z.; Hu, W. *Adv. Mater.* **2013**, *25*, 6158.
- (22) Graham, K. R.; Cabanatos, C.; Jahnke, J. P.; Idso, M. N.; Labban, A. L.; Ndjawa, G. O. N.; Heumueller, T.; Vandewal, K.; Salleo, A.; Chmelka, B. F.; Amassian, A.; Beaujuge, P. M.; McGehee, M. D. *J. Am. Chem. Soc.* **2014**, *136*, 9608.
- (23) (a) Yuan, Q.; Mannsfeld, S. C. B.; Tang, M. L.; Toney, M. F.; Lüning, J.; Bao, Z. *J. Am. Chem. Soc.* **2008**, *130*, 3502. (b) Gann, E.; Gao, X.; Di, C.-a.; McNeill, C. R. *Adv. Funct. Mater.* **2014**, DOI: 10.1002/adfm.201401228.
- (24) (a) Jackson, N. E.; Savoie, B. M.; Kohlstedt, K. L.; Marks, T. J.; Chen, L. X.; Ratner, M. A. *Macromolecules* **2014**, *47*, 987. (b) Perez, L. A.; Zalar, P.; Ying, L.; Schmidt, K.; Toney, M. F.; Nguyen, T.-Q.; Bazan, G. C.; Kramer, E. J. *Macromolecules* **2014**, *47*, 1403. (c) Ying, L.; Hsu, B. B. Y.; Zhan, H.; Welch, G. C.; Zalar, P.; Perez, L. A.; Kramer, E. J.; Nguyen, T.-Q.; Heeger, A. J.; Wong, W.-Y.; Bazan, G. C. *J. Am. Chem. Soc.* **2011**, *133*, 18538.
- (25) Gao, X.; Hu, Y. *J. Mater. Chem. C* **2014**, *2*, 3099.
- (26) Najari, A.; Beaupré, S.; Berrouard, P.; Zou, Y.; Pouliot, J.-R.; Lepage-Pérusse, C.; Leclerc, M. *Adv. Funct. Mater.* **2011**, *21*, 718.
- (27) Kirby, N. M.; Mudie, S. T.; Hawley, A. M.; Cookson, D. J.; Mertens, H. D. T.; Cowieson, N.; Samardzic-Boban, V. *J. Appl. Crystallogr.* **2013**, *46*, 1670.